2019-05-23

DFIB-SPH study of submerged horizontal cylinder oscillated close to the free surface of a viscous liquid

Moballa, B

10.1088/1873-7005/ab1893
Fluid Dynamics Research
IOP Publishing

DFIB-SPH Study of Submerged Horizontal Cylinder Oscillated Close to The Free Surface of a Viscous Liquid

Burniadi Moballa[1], Ming-Jyh Chern[1]‡, Avicenna An-Nizhami[1] and A G L Borthwick[2]

[1]Department of Mechanical Engineering, National Taiwan University of Science and Technology, Taipei 10607, TAIWAN

[2]School of Engineering, The University of Edinburgh, Edinburgh EH9 3JL, UK

E-mail: mjchern@mail.ntust.edu.tw

Abstract. The hydrodynamics is studied numerically of a horizontal cylinder undergoing forced in-line oscillation beneath the free surface of otherwise quiescent liquid at low Keulegan-Carpenter and Froude numbers. The DFIB-SPH numerical model uniquely combines two well-established techniques: the direct forcing immersed boundary (DFIB) method and smoothed particle hydordynamics (SPH). This facilitates accurate evaluation of the potentially violent free surface motions through SPH and the hydrodynamic force on the solid body using a volume integral. A parameter study is conducted covering a range of Keulegan-Carpenter numbers (KC = 3, 7, and 10) and submergence ratios ($H/D = 0.5 - 2.0$) at fixed Reynolds number (Re = 100) and Froude number (Fr = 0.35). The flow pattern and transverse force coefficient are found to be affected by the proximity of the cylinder to the free surface. Spectral analysis suggests that free surface wave motions are linked to the transverse force acting on the submerged, oscillating cylinder.

Keywords: Smoothed Particle Hydrodynamics (SPH), Direct forcing immersed boundary method, Solid-fluid interaction, Weakly compressible, δ-SPH, Oscillating cylinder, Free surface

‡ Corresponding author: mjchern@mail.ntust.edu.tw

1. Introduction

Accurate prediction of fluid-structure interaction is important in the design of offshore structures, the majority of which consist of assemblages of cylindrical members. Oscillating horizontal cylinder in otherwise quiescent fluid represents a simplified model of the vibration of horizontal cylindrical member of an offshore structure. It also provides a simple model of vibrating tube or pipe submerged in liquid inside a tank or vessel.

Flow around an oscillating cylinder in quiescent fluid is characterised by two non-dimensional numbers, the Keulegan-Carpenter number (KC = $\frac{UT}{D}$) and Reynolds number (Re = $\frac{UD}{\nu}$) where U is the velocity amplitude, T is the period of cylinder oscillation, D is the cylinder diameter, and ν is the fluid kinematic viscosity coefficient. The ratio between KC and Re is called the frequency parameter, and denoted as

$$\beta = \frac{\mathrm{Re}}{\mathrm{KC}}. \tag{1}$$

Many researchers have studied vortex formation in the vicinity of a stationary cylinder in oscillatory flow or an oscillating cylinder in otherwise quiescent fluid. A systematic description of the vortex formation pattern is given by Williamson (1985) who grouped the flow regimes according to the KC number, namely: pairing of attached vortices ($0 < \mathrm{KC} < 7$), transverse street/single-pair ($7 < \mathrm{KC} < 15$), double-pair ($15 < \mathrm{KC} < 24$), three-pair ($24 < \mathrm{KC} < 32$), and four-pair ($32 < \mathrm{KC} < 40$). A subsequent study by Obasaju *et al* (1988) observed similar flow regimes and boundaries between regimes in terms of KC. Obasaju *et al* (1988) named the double-pair as the diagonal regime, the three-pair as the third vortex regime, and the higher regimes as the quasi-steady regime. For $0 < \mathrm{KC} < 7$, a pair of vortices forms in the cylinder wake and remains attached to the cylinder each half cycle. The attached vortex pair is symmetric up to $\mathrm{KC} = 4$. In the symmetric regime, the fundamental frequency of in-line force is equal to the frequency of cylinder oscillation, and the transverse force is virtually zero. For $\mathrm{KC} > 4$, the vortex pair becomes asymmetric giving rise to a fluctuating transverse force at the oscillation frequency. In the transverse street/single-pair regime, a vortex is shed from the cylinder each half cycle. During two successive half cycles, two vortices of opposite sign are released. A vortex street develops with time in the direction of vortex migration. At $7 < \mathrm{KC} < 13$, the vortices migrate in a direction roughly perpendicular to the cylinder movement. At $13 < \mathrm{KC} < 15$, the vortex pair advects away at about 45^o to the direction of cylinder oscillation. In the single-pair regime, the fundamental frequency of the transverse force is twice the frequency of cylinder oscillation whereas the in-line force continues to fluctuate at the same frequency as the cylinder oscillation. The higher regimes is named according to the number of vortex pair sheds each cycle. For each flow regime, Williamson (1985) found that the ratio of frequency of transverse force and cylinder oscillation is constant over the range of β value studied. It should be noted however, that an earlier study by Sarpkaya at higher Reynolds number suggested that the ratio increases progressively with increasing frequency parameter (Sumer and Fredsøe, 2006). The investigations by Williamson (1985) and Obasaju *et al* (1988) were

conducted at a relatively high value of frequency parameter. Tatsuno and Bearman (1990) mapped flow regimes at a low frequency parameter ($\beta < 160$) for KC < 15). They found eight distinct flow regimes in terms of KC and β. Numerical investigations conducted later by Justesen (1991) and Iliadis and Anagnostopoulos (1998) using two-dimensional models confirmed the flow pattern identified in the foregoing experimental results and revealed that the inception of asymmetric flow is a function of β.

Most studies concerning an oscillating cylinder in otherwise quiescent fluid or oscillatory flow past a stationary cylinder consider a cylinder placed in an infinite fluid or very far from the boundary. Relatively few studies have been conducted to investigate the effect of proximity to a boundary which can act to suppress vortex shedding. In a study of the effect of wall proximity in oscillatory flows, Sumer *et al* (1991) found that the vortex shedding regimes identified by Williamson (1985) can change considerably. At KC = 4, the symmetry of the attached vortex pair disappears with decreasing gap ratio, the ratio of the distance from the cylinder to the bottom wall boundary and the cylinder diameter. For zero gap ratio, the attached vortex only grows from the top surface of the cylinder. Because of proximity to the wall, the vortex from the previous half cycle is swept over the top surface of the cylinder and disappears during the start of the next half cycle. The transverse vortex street, observed by Williamson (1985) for $7 <$ KC < 13, disappears for gap ratio < 1.7, for which the line of migration of the vortex pair is parallel to the free stream. This vortex pattern is confirmed by Scandura *et al* (2009) who undertook numerical simulation for KC = 10 and $\beta = 20$ and 50. At small KC, such as 10-20, vortex shedding is maintained for gap ratios down to about 0.1. The critical value of the gap ratio, a value below which the vortex shedding is suppressed, increases with KC.

Lin and Rockwell (1999) studied experimentally the effect of proximity to the free surface on the hydrodynamic force on a submerged body at very low Fr and constant KC = 10. They found that for a cylinder placed relatively far from the free surface, two cycles of modulated transverse force occurred for each cycle of cylinder oscillation, in agreement with the established result for a cylinder in infinite fluid. The time history of transverse force matched that obtained by Obasaju *et al* (1988) also at KC = 10. Lin and Rockwell (1999) conducted their study at very low Fr number where the free surface only deforms slightly and the proximity effect is similar to that for a free slip boundary. At larger Fr, the free surface can undergo considerable deformation and wave breaking may occur, leading to substantial production of vorticity. To the present authors' knowledge, the effect of free surface vorticity on vortex formation at the cylinder remains largely unaddressed.

Smoothed particle hydrodynamics (SPH) (Monaghan 1994) offers a means of accurately simulating the violent free surface motions of a liquid. However, when SPH is applied to a submerged solid, it can be awkward to obtain a correct prediction of the hydrodynamic force, owing to the oscillatory pressure field and difficulty in enforcing non-slip boundary condition at the solid-liquid interface. Given that SPH evaluates pressure using an equation of state, the effect of the oscillating of pressure field can be

remedied by means of the δ-SPH method which introduces an additional density filter term to the continuity equation (Marrone *et al* 2011). However, the δ-SPH method employs an elaborate algorithm to evaluate field variables at the boundary based on moving least-squares interpolation (Marrone *et al* 2011).

The direct forcing immersed boundary method has been specifically developed to model fluid flow interactions with complicated immersed bodies (Noor *et al* 2009). By introducing a virtual force to the Navier-Stokes equation to enforce the non-slip boundary condition, the DFIB method eliminates the need for a boundary algorithm. The hydrodynamic force is then evaluated by means of a volume integral of the virtual force over the solid body, instead of the conventional surface integral of fluid stress which requires knowledge of boundary normal (Noor *et al* 2009).

In the present study, we apply a combination of direct forcing immersed boundary and smoothed particle hydrodynamics methods to study the local hydrodynamics induced by a submerged horizontal cylinder undergoing forced oscillations close to a liquid free surface at low Fr and KC. The DFIB method (based on the volume of solid function proposed by Noor *et al*) is used to model the solid body and simplify the hydrodynamic force calculation. For the SPH part, the δ-SPH method proposed by Marrone *et al*, which offers reduced noise in the pressure field, is implemented. In this manner, we exploit the best features of each technique. A parameter study is conducted for different submergence ratios (the ratio of the distance from the cylinder to the free surface and the cylinder diameter) and KC values, for constant Re and Fr. The effects are interpreted of submergence ratio and KC on the vortex pattern, the hydrodynamic force signature, and the free surface elevation.

2. Governing equations and numerical scheme

The SPH method uses a weakly compressible model to simulate an incompressible fluid. Therefore, instead of enforcing an incompressibility condition, we solve the continuity equation which is given in non-dimensional form as

$$\frac{\mathrm{D}\rho}{\mathrm{D}t} = -\rho\nabla\cdot\mathbf{u} \tag{2}$$

where ρ is non-dimensional density, t is non-dimensional time, and $\mathbf{u}$ is the non-dimensional velocity vector. The non-dimensional momentum conservation equation including the virtual force term, $\mathbf{f}$, defined by the DFIB method can be written as

$$\frac{\mathrm{D}\mathbf{u}}{\mathrm{D}t} = -\frac{1}{\rho}\nabla p + \frac{1}{\mathrm{Re}}\nabla^2\mathbf{u} + \mathbf{g} + \mathbf{f} \tag{3}$$

where p is non-dimensional pressure and $\mathbf{g}$ is the non-dimensional body force term given as $\mathbf{g} = \left(0\mathbf{i} + \frac{-1}{\mathrm{Fr}^2}\mathbf{j}\right)$. Here, the Froude number is based on the cylinder diameter and defined as $\mathrm{Fr} = U/\sqrt{gD}$ where g is the gravitational acceleration. In the weakly compressible model, the pressure is obtained from the following linear equation of state,

$$p = c_0^2\left(\rho - 1\right) \tag{4}$$

where c_0 is the non-dimensional reference speed of sound.

To smooth the pressure field, a filter is applied, based on inclusion of a density diffusion term, in keeping with the δ-SPH method. With this additional term, the semi-discrete continuity equation reads

$$\frac{\mathrm{D}\rho_i}{\mathrm{D}t} = -\rho_i \sum_j (\mathbf{u}_j - \mathbf{u}_i) \cdot \nabla_i \tilde{W}_{ij} V_j + \delta h c_0 \sum_j \boldsymbol{\psi}_{ij} \cdot \nabla_i \tilde{W}_{ij} V_j \tag{5}$$

where i denotes the ith particle, j denotes a neighbouring particle, $\nabla_i \tilde{W}_{ij}$ is the corrected gradient of the kernel function, δ is a coefficient that represents the intensity of diffusion, h is the support length of the kernel function, $\boldsymbol{\psi}_{ij}$ is the density diffusion term, and V_j is the volume of the jth neighbour particle. In this study, $\delta = 0.1$. The density diffusion term, $\boldsymbol{\psi}_{ij}$, is given by

$$\boldsymbol{\psi}_{ij} = 2\frac{(\rho_j - \rho_i)}{|\mathbf{x}_{ij}|}\frac{\mathbf{x}_{ij}}{|\mathbf{x}_{ij}|} - (\nabla\rho_i + \nabla\rho_j) \tag{6}$$

where $\mathbf{x}_{ij} = \mathbf{x}_j - \mathbf{x}_i$, and $\mathbf{x}$ is the position vector. The semi-discrete Navier-Stokes equation can be written as

$$\begin{aligned}\frac{\mathrm{D}\mathbf{u}_i}{\mathrm{D}t} = &-\sum_j m_j \left(\frac{p_i}{\rho_i^2} + \frac{p_j}{\rho_j^2}\right) \nabla_i \tilde{W}_{ij} \\ &+ \frac{2}{\mathrm{Re}} \left[\sum_j (\mathbf{u}_j - \mathbf{u}_i) \left(\frac{\mathbf{x_{ij}}}{|\mathbf{x}_{ij}|^2} - \sum_j \nabla_i W_{ij} V_j\right) \cdot \nabla_i \tilde{W}_{ij} V_j\right] \cdot \\ &+ \mathbf{g} + \mathbf{f}_i\end{aligned} \tag{7}$$

In Eq. (7), the pressure gradient term is discretized using a symmetric gradient operator and the viscous term is discretized using a Laplacian operator similar to the one proposed by Schwaiger (2008). The corrected kernel gradient at the ith particle, $\nabla_i \tilde{W}_{ij}$, in Eqs. (5) and (7) is given by

$$\nabla_i \tilde{W}_{ij} = \mathbf{L}_i \cdot \nabla_i W(\mathbf{x}_{ij}) \tag{8}$$

where $\mathbf{L}_i$ is the kernel gradient correction proposed by Chen *et al* (1999) and W_{ij} is the quintic Wendland kernel function. In the present study, the smoothing length of the kernel function is $1.2\Delta x_0$ where Δx_0 is the initial particle spacing.

The virtual force term in Eq. (7) is defined as

$$\mathbf{f}_i = \eta_i \frac{\mathbf{u}_s - \mathbf{u}_i}{\Delta t} \tag{9}$$

where η_i is the volume of solid (VOS) function of the ith particle and $\mathbf{u}_s$ is the prescribed solid velocity (Noor *et al* 2009). This term represents the interaction between the solid and fluid. Inclusion of this term in the Navier-Stokes equation enforces the non-slip boundary condition on the solid body. For a regular geometry, such as a circular cylinder, η_i can be represented by an analytical equation. For a circular cylinder, the formula is

$$\eta_i(x_i, y_i) = \begin{cases} 1 & \text{for } \sqrt{(x_i - x_C)^2 + (y_i - y_C)^2} \leq r \\ 0 & \text{otherwise,} \end{cases} \tag{10}$$

where x_C and y_C are the coordinate of the center of the cylinder and r is the radius of the cylinder. In the grid-based method, the solid boundary does not generally coincide with the cell. Therefore, the volume of solid function does not exactly represent the solid geometry. Consequently, the non-slip boundary condition is enforced slightly inside the solid boundary. This problem can be remedied by using smaller grid around the solid body. In the SPH method, this problem can be avoided by uniformly distributing some particles inside the solid region and also along the solid boundary. The hydrodynamic force is calculated using a volume integral of the virtual force given as

$$\mathbf{F} = -\int \mathbf{f} \mathrm{d}m \tag{11}$$

which is easier to evaluate than the conventional surface integral. For the SPH method, the above formula can be discretized into summation over the fluid particles.

In the WCSPH model, the density variation needs to be restricted in order that the fluid behaves properly as it approaches the incompressibility limit. This is achieved by prescribing the reference speed of sound, c_0, in the equation of state such that the Mach number is less than or equal to 0.1 ($\mathrm{M} \leq 0.1$). Therefore, it is customary in the WCSPH model, to set

$$c_0 \geq 10 U_{max} \tag{12}$$

where U_{max} is the maximum velocity. If the body force is absent, U_{max} can be chosen equal to the inlet velocity or the boundary velocity (for cases with a moving boundary such as the cavity flow). When a body force is present, the maximum velocity is selected as

$$U_{max} = \sqrt{\frac{L}{\mathrm{Fr}^2}} \tag{13}$$

where L is the initial fluid depth.

In the present study, the bottom boundary is modelled using dynamic boundary particles (Crespo and Dalrymple, 2007). Instead of using an open or periodic boundary condition at a vertical boundary, we use a wall boundary with a numerical damping layer placed in front of it. The damping layer slowly brings the velocity to the far field value of zero. Here the damping model is applied in a similar way to that of Mayer *et al* (1998) using the decay function suggested by Fuhrman *et al* (2006). Fig. 1 depicts schematically the problem domain and the damping zones.

Time integration is carried out using the predictor-corrector Beeman algorithm. Virtual force is omitted when calculating the acceleration in both prediction and correction steps of the Beeman algorithm. The predictor step is

$$\mathbf{u}_i^* = \mathbf{u}_i^n + \frac{1}{2}\Delta t \left(3\mathbf{a}_i^n - \mathbf{a}_i^{n-1}\right), \tag{14}$$

$$\rho_i^* = \rho_i^n + \frac{1}{2}\Delta t \left(3\dot{\rho}_i^n - \dot{\rho}_i^{n-1}\right), \text{ and} \tag{15}$$

$$\mathbf{x}_i^* = \mathbf{x}_i^n + \left[\Delta t \mathbf{u}_i^n + \frac{1}{6}\Delta t^2 \left(4\mathbf{a}_i^n - \mathbf{a}_i^{n-1}\right)\right](1 - \eta_i) \tag{16}$$

where $\mathbf{a} = \frac{\mathrm{D}\mathbf{u}}{\mathrm{D}t}$ and $\dot{\rho} = \frac{\mathrm{D}\rho}{\mathrm{D}t}$. The predicted pressure is calculated as

$$p_i^* = c_0^2 \left(\rho_i^* - 1\right) \tag{17}$$

The corrector step is based on the Adam-Bashforth-Moulton method and is given by

$$\mathbf{u}_i^{**} = \mathbf{u}_i^n + \frac{1}{12}\Delta t \left(5\mathbf{a}_i^* + 8\mathbf{a}_i^n - \mathbf{a}_i^{n-1}\right), \tag{18}$$

$$\rho_i^{n+1} = \rho_i^n + \frac{1}{12}\Delta t \left(5\dot{\rho}_i^* + 8\dot{\rho}_i^n - \dot{\rho}_i^{n-1}\right), \text{ and} \tag{19}$$

$$\mathbf{x}_i^{**} = \mathbf{x}_i^n + \left[\Delta t \mathbf{u}_i^n + \frac{1}{6}\Delta t^2 \left(\mathbf{a}_i^* + 2\mathbf{a}_i^n\right)\right](1 - \eta_i). \tag{20}$$

The pressure is updated by

$$p_i^{n+1} = c_0^2(\rho_i^{n+1} - 1). \tag{21}$$

Next, an equation of motion is solved for the solid velocity, $\mathbf{u}_s^{n+1}$, and displacement, $\Delta\mathbf{x}_s^{n+1}$. Subsequently, the virtual force is updated by

$$\mathbf{f}_i^{n+1} = \eta_i \frac{\mathbf{u}_s^{n+1} - \mathbf{u}_i^{**}}{\Delta t}. \tag{22}$$

Finally, the fluid velocity is corrected using the updated virtual force,

$$\mathbf{u}_i^{n+1} = \mathbf{u}_i^{**} + \Delta t\, \mathbf{f}_i^{n+1}, \tag{23}$$

and the position of fluid particle is updated by

$$\mathbf{x}_i^{n+1} = \mathbf{x}_i^{**} + \Delta\mathbf{x}_s^{n+1}\eta_i. \tag{24}$$

After the time integration step, the velocity of the fluid particles in the damping zone is corrected according to the damping model. A variable time step is used, following Monaghan and Kos (1999). The numerical scheme described above is implemented by modifying the open-source SPHYSICS code (Gomez-Gesteira *et al* 2012). The code is compiled and run on Intel® Xeon® E5-2650 processors and Linux environment.

3. Results and discussion

The implemented numerical scheme is first validated and tested for particle number independence by simulating the forced oscillations of a horizontal cylinder in otherwise quiescent fluid without a free surface at low KC. The cylinder is oscillated sinusoidally, with velocity prescribed by

$$u_s(t) = -\cos(2\pi f_0 t). \tag{25}$$

Fig. 1 shows the problem domain. Results are then presented from a parameter study for KC = 3, 7, and 10 and submergence ratio values of $H/D = 0.5$, 0.75, 1.0, 1.5, and 2.0 at constant Re = 100 and Fr = 0.35.

3.1. Validation and particle independence

The DFIB-SPH model is validated for the case of a cylinder oscillated in an infinite expanse of otherwise still fluid (i.e. without a free surface) at KC = 5 and Re = 100. At such low KC and Re, it is well established that vortices form, grow, and then remain attached to the cylinder. The present numerical predictions are compared against experimental data and alternative numerical prediction obtained using a finite volume solver with a body fitted grid by Dütsch *et al* (1998). Fig. 2 shows the predicted limit-cycle time histories of transverse force over three oscillation cycles obtained for three different smoothed particle sizes against corresponding numerical predictions presented by Dütsch *et al* (1998); it should be noted that the DFIB-SPH results in Fig. 2 have been post-processed using a method recommended by Shen *et al* (2009). The present results are in agreement with those of Dütsch *et al* especially for $\Delta x_0 = 0.04D$ and $\Delta x_0 = 0.025D$ where grid convergence appears to have been achieved. We therefore use $\Delta x_0 = 0.04D$ for the subsequent cases. Fig. 3 depicts the present predictions and Dütsch *et al*'s experimental measurements of vertical profiles of horizontal (left column) and vertical (right column) velocity components at time $t = nT + 7T/12$ (corresponding to a phase angle of 210^o) at three sections in the stream-wise direction along the domain. The current position of the cylinder can be seen at section $x = 0.6$ where the horizontal velocity component is constant at about 0.8 and the vertical velocity component is constant at 0.0 for $-0.5 \leq y \geq 0.5$. In general, both sets of results are in very close agreement, the slight discrepancies arising because of the assumption of two-dimensional flow in the present model, unlike the fully three-dimensional experiments conducted by Dütsch *et al*.

3.2. Parameter study

A parameter study is now described using predictions made by the DFIB-SPH model to examine the influence of the distance to the free surface of a horizontal cylinder undergoing forced oscillations on the surrounding flow pattern, hydrodynamic force coefficients, and free surface wave deformation for KC = 3, 7, and 10. In all cases, the still water depth is set equal to $7D$, where D is the diameter of the cylinder. The submergence ratio H/D is expressed as the ratio of the depth of submergence from the still water level to the top of the cylinder, H, to the diameter of the cylinder, D.

3.2.1. Effect of submergence ratio on flow patterns First, we consider the submergence effect at a low value of KC = 3. For submergence ratio in the range $1.0 \leq H/D \leq 2.0$, an asymmetric vortex pair forms behind the cylinder. Fig. 4 illustrates the predicted instantaneous vorticity distribution in the plane of the cylinder at four intervals during the oscillation cycle for $H/D = 2.0$. As the cylinder reaches the end of a half cycle and reverses, a vortex pair detaches from the cylinder surface. A nascent vortex of opposite rotation forms on the other side of the cylinder, and as this vortex pair grows larger, the previously detached vortices disappear. The degree of asymmetry of the

vortex pair is different between the first half cycle and the second half cycle. During the first half cycle, when the cylinder moves towards the left, the degree of asymmetry in the vortex pair is smaller compared to the second half cycle when the cylinder moves towards the right. During the first half cycle, the upper vortex is slightly bigger and has higher absolute peak vorticity than the lower vortex. In the second half cycle the situation is reversed. The lower vortex is considerably bigger and has higher absolute peak vorticity. A similar flow pattern is observed when the cylinder is placed beneath a free surface at $H/D = 1.5$. When the cylinder is placed closer to the free surface, such that the submergence ratio becomes $H/D = 1.0$, the degree of asymmetry of the vortex pair becomes larger. At larger submergence ratios the highest vorticity keeps alternating between the upper and lower vortices but, at $H/D = 1.0$, the lower vortex is consistently larger compared to the upper vortex throughout the cycle. Whereas the lower vortex grows downstream, the upper vortex is swept over along the back surface of the cylinder. No vortex shedding occurs for $1.0 \leq H/D \leq 2.0$ at KC $= 3$. For $H/D = 0.5$ and 0.75, a transverse vortex street develops. At the smaller submergence ratios, the degree of asymmetry between the upper and lower vortices is larger, with the upper vortex curling further downward along the back surface of the cylinder. At the end of a half cycle, the upper vortex reaches the bottom of the cylinder and interacts with the lower vortex causing it to detach. The lower shed vortex then travels downward (perpendicular to the direction of cylinder oscillation). At the end of the following half cycle, another vortex with opposite sign is shed from the bottom of the cylinder. At a submergence ratio of 0.5, free surface wave breaking occurs downstream of the cylinder, generating a vortex which advects downward to the cylinder and coalesces with the attached upper vortex on the cylinder surface, substantially increasing the strength of the upper vortex (see Fig. 5).

At the higher value of KC $= 7$, an asymmetric vortex pair again forms behind the cylinder during each half cycle at submergence ratio $H/D = 1.0$, 1.5, and 2.0. Fig. 6 depicts the vorticity pattern over a complete limit cycle for $H/D = 1.0$. The lower vortex is always larger than the upper vortex. At the end of each half cycle, a vortex is shed from the bottom of the cylinder. When the cylinder reverses, instead of advecting away from the cylinder and helping to form a vortex street, the shed vortex is washed back towards the cylinder and its energy dissipated. The process effectively repeats itself, but in an alternating direction, each half cycle. It should be noted that KC ≈ 7 represents the transition from attached vortices (for KC < 7) to vortex shedding (for KC > 7) regimes observed for a cylinder oscillated far from any boundary (Obasaju *et al* 1988). At a lower submergence value of $H/D = 0.75$, vortex shedding occurs forming a transverse street. At KC $= 7$, the shed vortex does not travel far, but instead dissipates after advecting downward at about $1D$. At the free surface, wave breaking starts to occur behind the cylinder, and a vortex is released from the breaker that advects toward the cylinder. The vortex shedding and wave breaking processes are similar to those at KC $= 3$ and $H/D \leq 0.75$. A similar flow pattern is also observed at KC $= 7$ and $H/D = 0.5$, where the shed vortex is stronger and so advected further downward,

helping form a vortex street. At the free surface, wave breaking, vorticity production, and vortex merging phenomena similar to the $H/D = 0.75$ are observed.

At KC = 10, a single asymmetric vortex pair is again observed at submergence ratios $H/D = 1.0$, 1.5, and 2.0, with similar behaviour as noted for KC = 3 and 7 at the same values of submergence ratio. A single-pair regime is observed at KC = 10 and $H/D = 0.75$ (see Fig. 7). At the end of the first half cycle during which the cylinder moves to the left, a negative (clockwise-rotating) lower vortex is shed from the bottom of the cylinder. This lower vortex is similar to that which develops in the washed back shedding regime, but is much stronger. Hence, when the cylinder moves to the right during the second half cycle, instead of being washed back and dissipating, the detached lower vortex advects below the cylinder to the left. At the end of the second half cycle, a positive-signed lower vortex is shed from the bottom of the cylinder. The newly shed vortex forms a pair with its predecessor. This vortex pair then advects downward at an angle to the direction of cylinder oscillation, but does not persist long; the lower vortex from the first half cycle decays slowly eventually disappearing as does its successor. An upper vortex is also detached at the end of each half cycle. However, the upper shed vortex is almost immediately washed back towards the cylinder and reattaches, helping form the lower vortex during flow reversal. During each half cycle, wave breaking is also observed behind the moving cylinder. Wave breaking produces vorticity at the free surface, leading to the generation of a vortex when the cylinder reverses direction, and the disturbance to the free surface stops. This vortex advects downward towards the cylinder and merges with a vortex of the same sign on the surface of the cylinder. At $H/D = 0.5$, the breaking of free surface waves intensifies, creating a stronger upper vortex which remains attached, migrating around the back of the cylinder to its base (see Fig. 8). This process forces the lower shed vortex to migrate downward (perpendicular to the cylinder movement) causing a transverse vortex to form.

Fig. 9 maps the flow patterns observed in the present study according to Keulegan-Carpenter number and submergence ratio. A trend is noticeable that departs from the infinite fluid and near wall cases. In the case of an oscillating cylinder in infinite fluid, the flow pattern is entirely determined by KC, whereas in the case of an oscillating cylinder in a liquid with a free surface, the flow pattern is also affected by the proximity of the cylinder to the free surface. Sumer *et al* (1991) studied the effect of a plane boundary on oscillatory flow past a cylinder and found that the wall boundary consistently acts to suppress vortex formation and shedding across all KC numbers. Our predictions of free surface, viscous flow past a cylinder show that the free surface plays a different role to that of a fixed wall. At low values of KC, proximity of the cylinder to the liquid free surface tends to promote vortex shedding, whereas there is no shedding in the case of infinite fluid. At higher values of KC, the free surface can act to promote a higher regime of vortex shedding pattern for small submergence ratio than for the infinite fluid case. At smallest cylinder submergence, the vortex shedding pattern reverts to the transverse street regime, indicating that strong wave breaking at the free surface confines vortex formation in the transverse street regime.

Unlike a plane wall boundary, free surface is deformable. As the distance between cylinder and still water level is reduced, the free surface flow over the cylinder becomes supercritical leading to a moving hydraulic jump becoming established downstream (relative to the direction of motion of the cylinder) whose wave amplitude grows until wave breaking occurs. The breaking wave produces considerable vorticity which interacts with the flow field immediately to the lee of the moving cylinder. It is this interaction that influences the flow patterns observed at the smallest submergence ratios considered herein.

3.2.2. Hydrodynamic force components We now examine the spectra of in-line and transverse force coefficients and free surface elevation time series, the latter computed vertically above the mean position of the oscillating cylinder. In all cases, the peak frequency of the in-line force coefficient is the same as the cylinder oscillation frequency, regardless the depth of submergence. Fig. 10 depict the in-line and transverse force coefficient spectrum along with the free surface elevation spectrum at KC = 3, 7, and 10 respectively, in each case for submergence ratios of 0.5, 1.0, and 2.0. At KC = 3, the peak transverse force frequency and peak free surface elevation spectral frequency occur at the cylinder oscillation frequency for $H/D = 1.0$ to 2.0, but alter to twice the cylinder oscillation frequency for $H/D = 0.5$, corresponding to vortex shedding. At KC = 7 and 10, the fundamental frequencies of the transverse force coefficient and free surface elevation spectra are invariably twice the frequency of cylinder oscillation for all submergence ratios. The general agreement between the peak frequencies of the transverse force coefficient and free surface elevation indicates an intimate coupling between the free surface motions and the underlying flow field which induces the transverse force on the cylinder.

Fig. 11 presents the root-mean-square of transverse force coefficient, $C_{l,rms}$, as a function of submergence ratio for KC = 3, 7, and 10. At a given value of Keulegan-Carpenter number, $C_{l,rms}$ increases as the submergence decreases; this is most pronounced for $1.0 \leq H/D \leq 2.0$ at KC = 3. At a given submergence, $C_{l,rms}$ increases as KC decreases. In short, $C_{l,rms}$ is a function of both KC and submergence ratio, experiencing the greatest variation as KC is reduced. Fig. 12 presents the corresponding plot of the average transverse force coefficient, $C_{l,avg}$, over the range of KC numbers and submergence ratios considered. Owing to the gravitational force component, $C_{l,avg}$ is negative for all KC numbers and submergence ratios. At constant KC, the magnitude of $C_{l,avg}$ decreases with increasing submergence until $H/D = 1.0$; for higher values of H/D, it seems that the free surface no longer affects the value of $C_{l,avg}$.

Fig. 13 shows the root-mean-square free surface displacement created by the oscillating cylinder as a function of cylinder submergence ratio for KC = 3, 7, and 10. Here we can see an almost linear, monotonic decline in root-mean-square free surface elevation with submergence ratio. There is less effect of KC, except that the root-mean-square free surface elevation is generally lower for KC = 7 than KC = 3 or 10.

4. Conclusions

A numerical model has been developed, based on a unique combination of otherwise well-established direct forcing immersed boundary (DFIB) and smoothed particle hydrodynamics (SPH) methods, for application to viscous free surface flows in the vicinity of solid boundaries. The model exploits the advantages of both methods, with DFIB used to evaluate boundary forces and SPH to represent the very complicated behaviour of a highly deformable liquid free surface. Particle convergence and validation tests have shown that the DFIB-SPH model accurately predicts the in-line forces and velocity profiles for a cylinder oscillated in almost infinite fluid at low Reynolds number, in agreement with published data from an alternative numerical model and laboratory experiments (Dütsch *et al* 1998). The DFIB-SPH model has been applied to a parameter study on the hydrodynamics of a cylinder forced to oscillate harmonically beneath the free surface of a viscous liquid, over ranges of KC numbers and submergence ratios at Re = 100 and Fr = 0.35. The model predictions indicate that the vorticity patterns depend on both KC and the proximity of the cylinder to the free surface. It is found that the free surface boundary has a different effect to a rigid-lid boundary, the latter suppressing vortex shedding. At low KC, where no vortex shedding is observed in the case of infinite fluid, the presence of a deformable free surface tends to promote vortex shedding at low values of cylinder submergence by supplying vorticity created by the breaking of a hydraulic jump wave that forms downstream of the crest of the cylinder. At higher KC, proximity of the cylinder to the free surface seems to confine the vortex shedding mode to a transverse vortex regime, arising from a strong vortex created within the breaking wave. It is also found that proximity to the free surface only affects the average transverse force coefficient when the submergence ratio is less or equal to the cylinder diameter. The magnitude of the transverse force coefficient and free surface elevation both increase as the cylinder's mean location approaches the free surface. The peak frequencies of the free surface elevation and transverse force coefficient time histories are consistently the same for any given KC and submergence ratio, which suggest that the free surface wave motions and transverse force on the oscillating cylinder are strongly coupled.

Acknowledgments

The authors would like to express their gratitude to the Ministry of Science and Technology, Taiwan for financial support through grants 103-2212-E-011-110-MY3 and 104-2511-S-011-005-MY3.

References

Chen J K, Beraun J E and Carney T C 1999 A corrective smoothed particle method for boundary value problems in heat conduction *Int. J. Numer. Methods Eng.* **46** 231–252

Crespo A J C and Dalrymple R A 2007 Boundary conditions generated by dynamic particles in SPH methods *C. Comput. Mater. Contin.* **5** 173–184

Dütsch H, Durst F, Becker S and Lienhart H 1998 Low-Reynolds-number flow around an oscillating circular cylinder at low Keulegan-Carpenter numbers *J. Fluid Mech.* **360** 249–271

Fuhrman D R, Madsen P A and Bingham H B 2006 Numerical simulation of lowest-order short-crested wave instabilities *J. Fluid Mech.* **563** 415–441

Gomez-Gesteira M, Rogers B, Crespo A, Dalrymple R, Narayanaswamy M and Dominguez J 2012 SPHysics – development of a free-surface fluid solver – Part 1: Theory and formulations *Comput. Geosci.* **48** 289–299

Iliadis G and Anagnostopoulos P 1998 Viscous oscillatory flow around a circular cylinder at low Keulegan-Carpenter numbers and frequency parameters *Int. J. Numer. Methods Fluids* **26** 403–442

Justesen P 1991 A numerical study of oscillating flow around a circular cylinder *J. Fluid Mech.* **222** 157–196

Lin J C and Rockwell D 1999 Horizontal oscillations of a cylinder beneath a free surface: vortex formation and loading *J. Fluid Mech.* **389** 1–26

Marrone S, Antuono M, Colagrossi A, Colicchio G,Le Touzé D and Graziani G 2011 δ-SPH model for simulating violent impact flows *Comput. Methods Appl. Mech. Eng.* **200** 1526–1542

Mayer S, Garapon A and Sørensen L S 1998 A fractional step method for unsteady free-surface flow with applications to non-linear wave dynamics *Int. J. Numer. Methods Fluids* **28** 293–315

Monaghan J 1994 Simulating free surface flows with SPH *J. Comput. Phys.* **110** 399–406

Monaghan J and Kos A 1999 Solitary waves on a Cretan beach *J. Waterw. Port, Coast. Ocean Eng.* **125** 145–154

Noor D Z, Chern M J and Horng T L 2009 An immersed boundary method to solve fluid-solid interaction problems *Comput. Mech.* **44** 447–453.

Obasaju E D, Bearman P W and Graham J M R 1988 A study of forces, circulation and vortex patterns around a circular cylinder in oscillating flow *J. Fluid Mech.* **196** 467–494

Scandura P, Armenio V and Foti E 2009 Numerical investigation of the oscillatory flow around a circular cylinder close to a wall at moderate Keulegan-Carpenter and low Reynolds numbers *J. Fluid Mech.* **627** 259–290

Schwaiger H F H 2008 An implicit corrected SPH formulation for thermal diffusion with linear free surface boundary conditions *Int. J. Numer. Methods Eng.* **75** 647–671

Shen L, Chan E S and Lin P 2009 Calculation of hydrodynamic forces acting on a submerged moving object using immersed boundary method *Comput. Fluids* **38** 691–702

Sumer B M and Fredsøe J 2006 *Hydrodynamics around cylindrical structures* (Singapore: World Scientific)

Sumer B M, Jensen B L and Fredsøe J 1991 Effect of a plane boundary on oscillatory flow around a circular-cylinder *J. Fluid Mech.* **225** 271–300

Tatsuno M and Bearman P W 1990 A visual study of the flow around an oscillating circular cylinder at low Keulegan-Carpenter numbers and low Stokes numbers *J. Fluid Mech.* **211** 157–182

Williamson C 1985 Sinusoidal flow relative to circular cylinders *J. Fluid Mech.* **155** 141–174

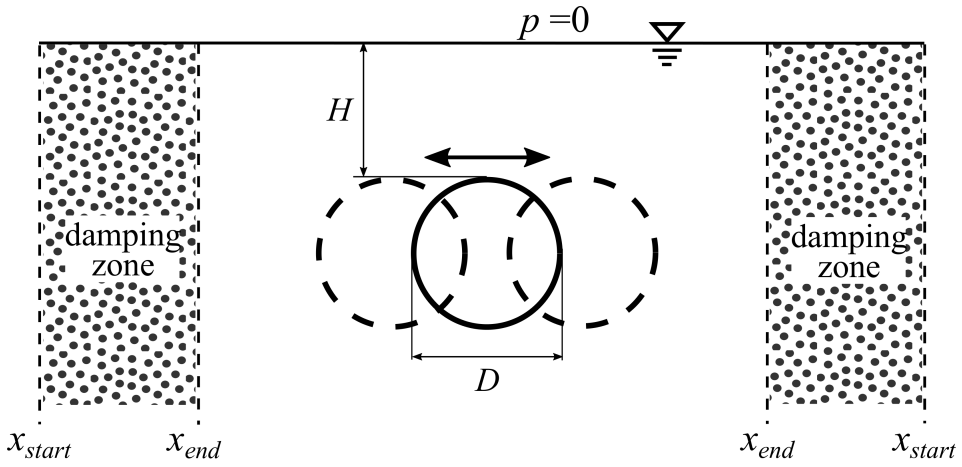

Figure 1. Problem domain.

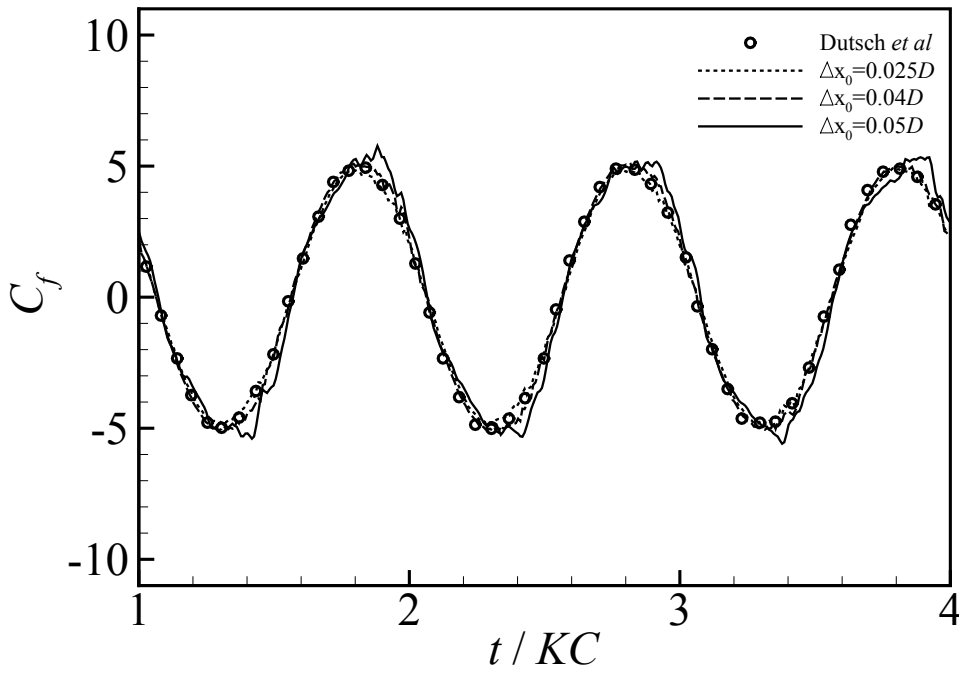

Figure 2. Validation and particle convergence test: time histories of in-line force coefficient obtained for a circular cylinder undergoing forced sinusoidal oscillations in otherwise still fluid at KC = 5 and Re = 100, obtained for three particle sizes using the DFIB-SPH model and experimentally by Dütsch *et al* (1998).

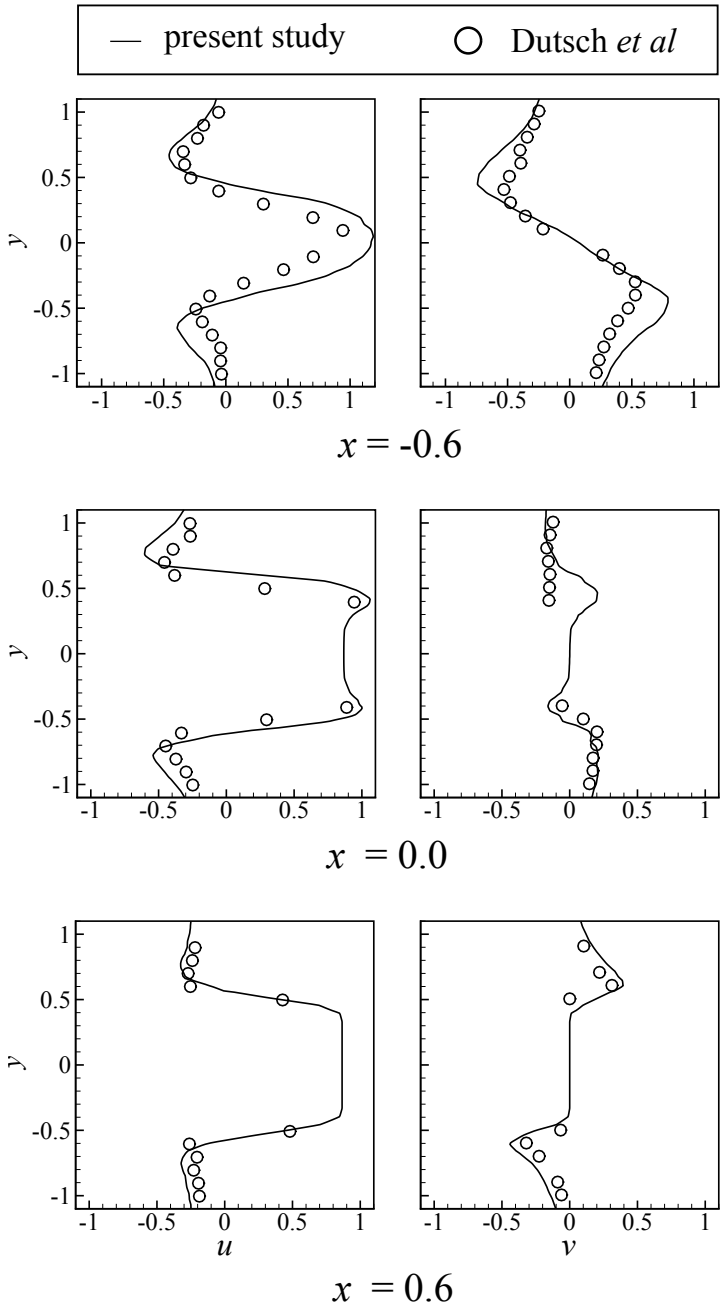

Figure 3. Non-dimensional vertical y-profiles of the in-line flow velocity component at three sections in the stream-wise direction along the domain, at time $t = nT + 7T/12$, corresponding to a phase angle of 210^o for KC $= 5$ and Re $= 100$: numerical predictions by the DFIB-SPH model, experimental data from Dütsch *et al* (1998).

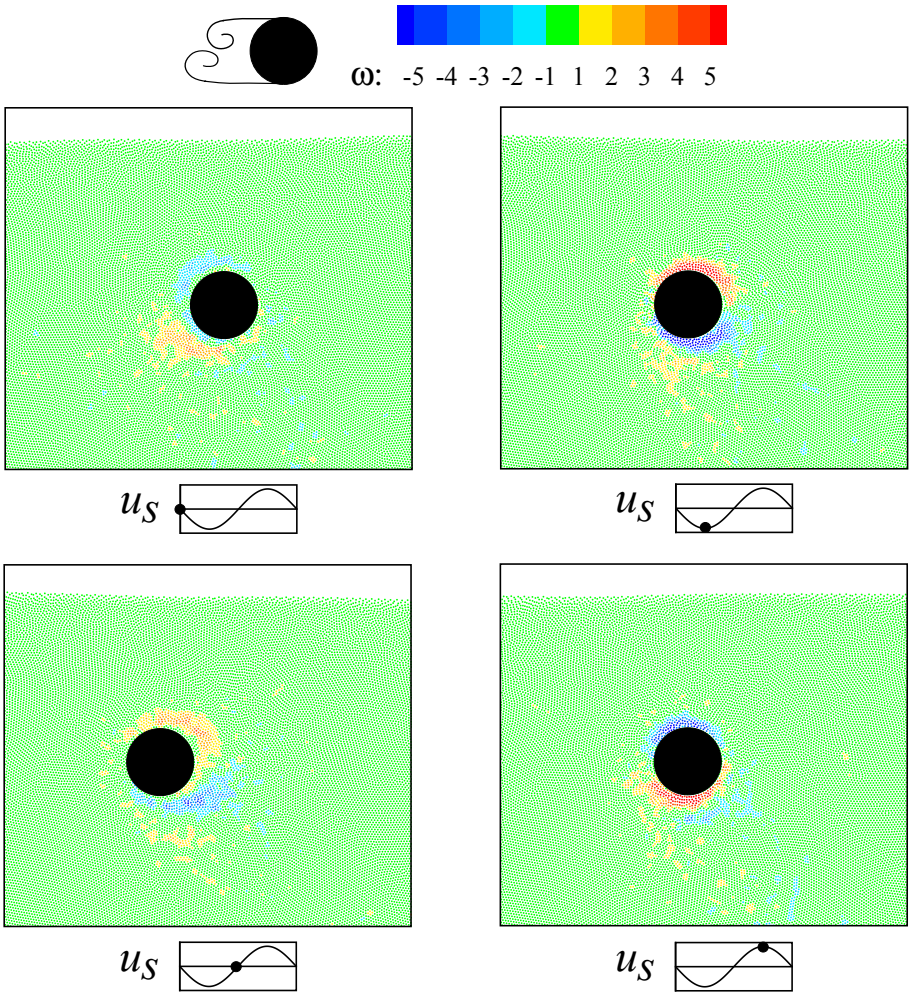

Figure 4. Instantaneous vorticity distribution predicted by the DFIB-SPH model at different times during the forced oscillation cycle of a horizontal cylinder beneath the free surface of a liquid for KC = 3, $H/D = 2.0$.

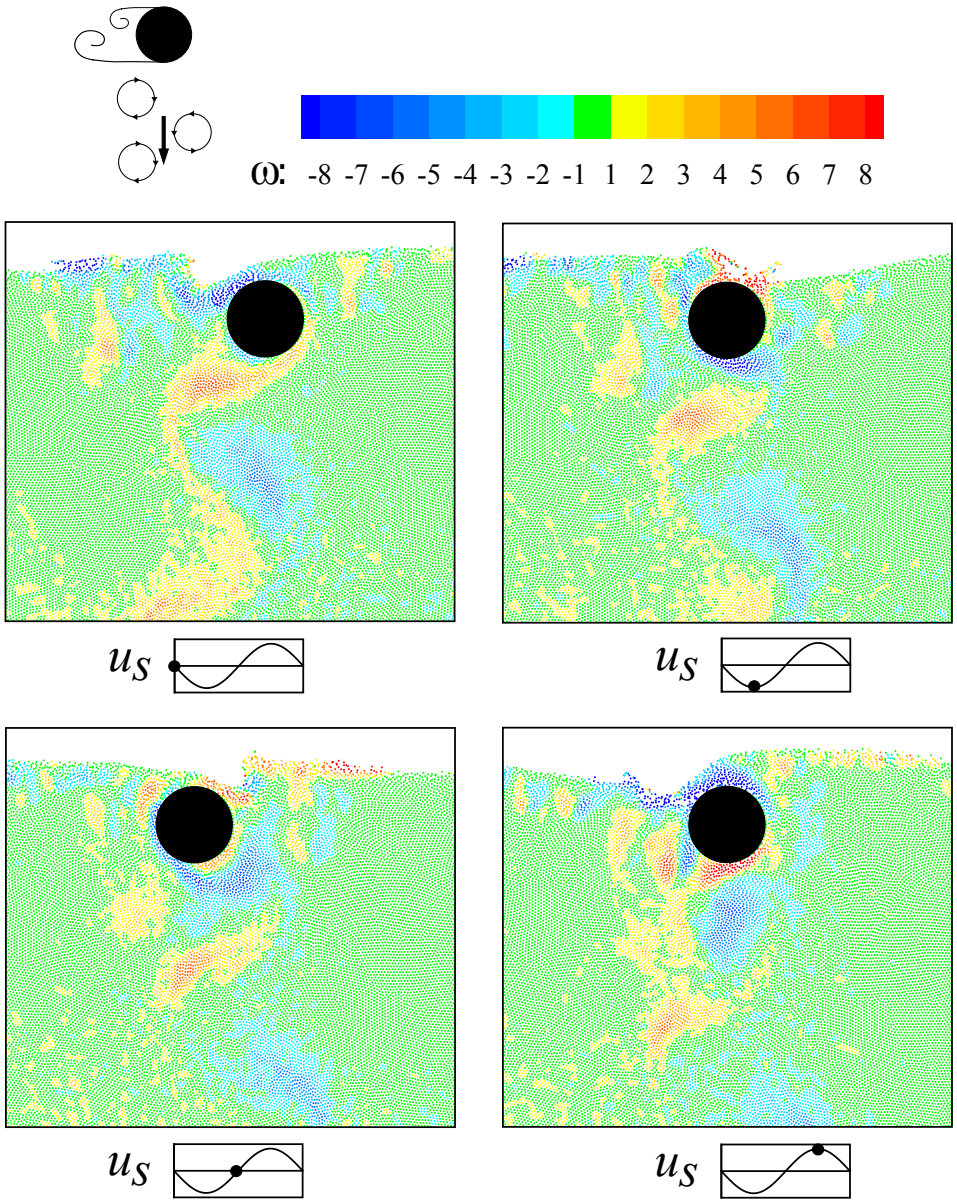

Figure 5. Instantaneous vorticity distribution predicted by the DFIB-SPH model at different times during the forced oscillation cycle of a horizontal cylinder beneath the free surface of a liquid for KC = 3, $H/D = 0.5$.

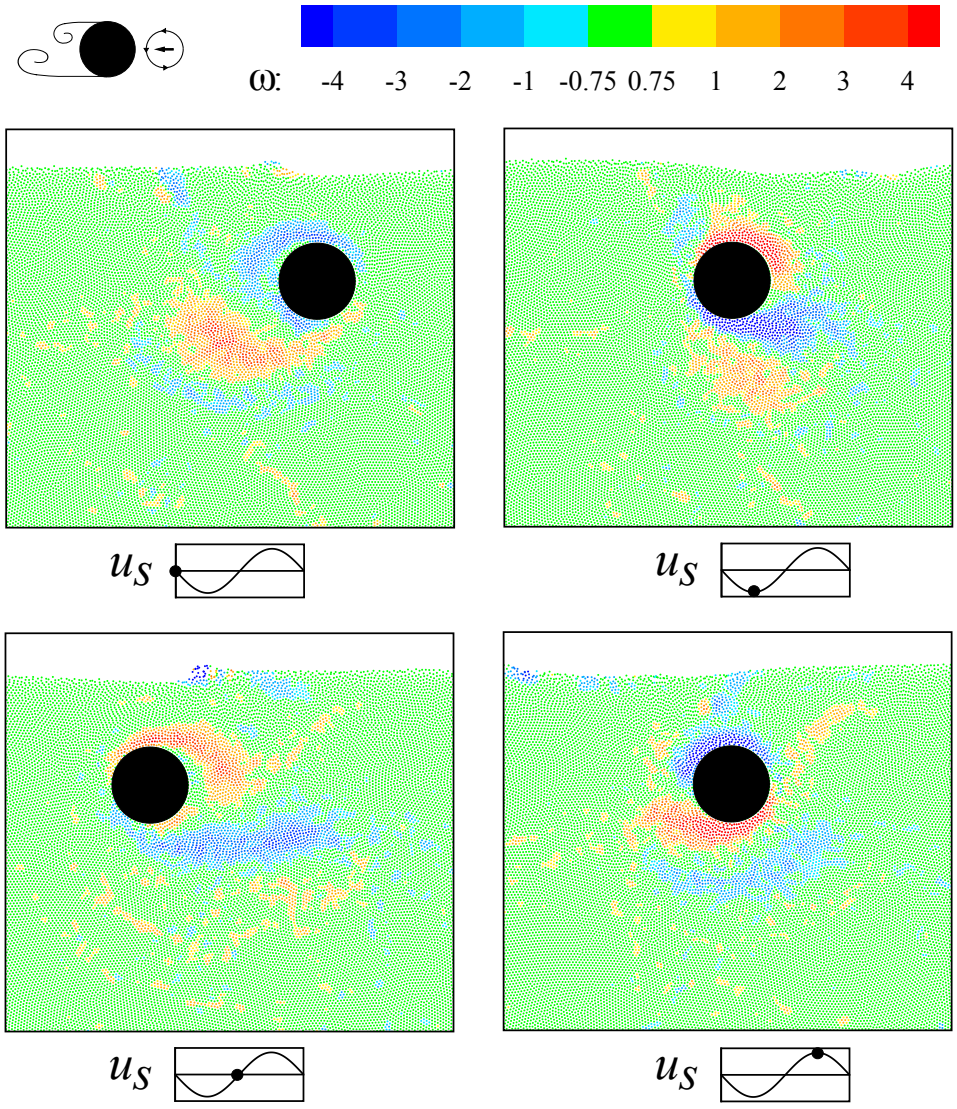

Figure 6. Instantaneous vorticity distribution predicted by the DFIB-SPH model at different times during the forced oscillation cycle of a horizontal cylinder beneath the free surface of a liquid for KC = 7 $H/D = 1.0$.

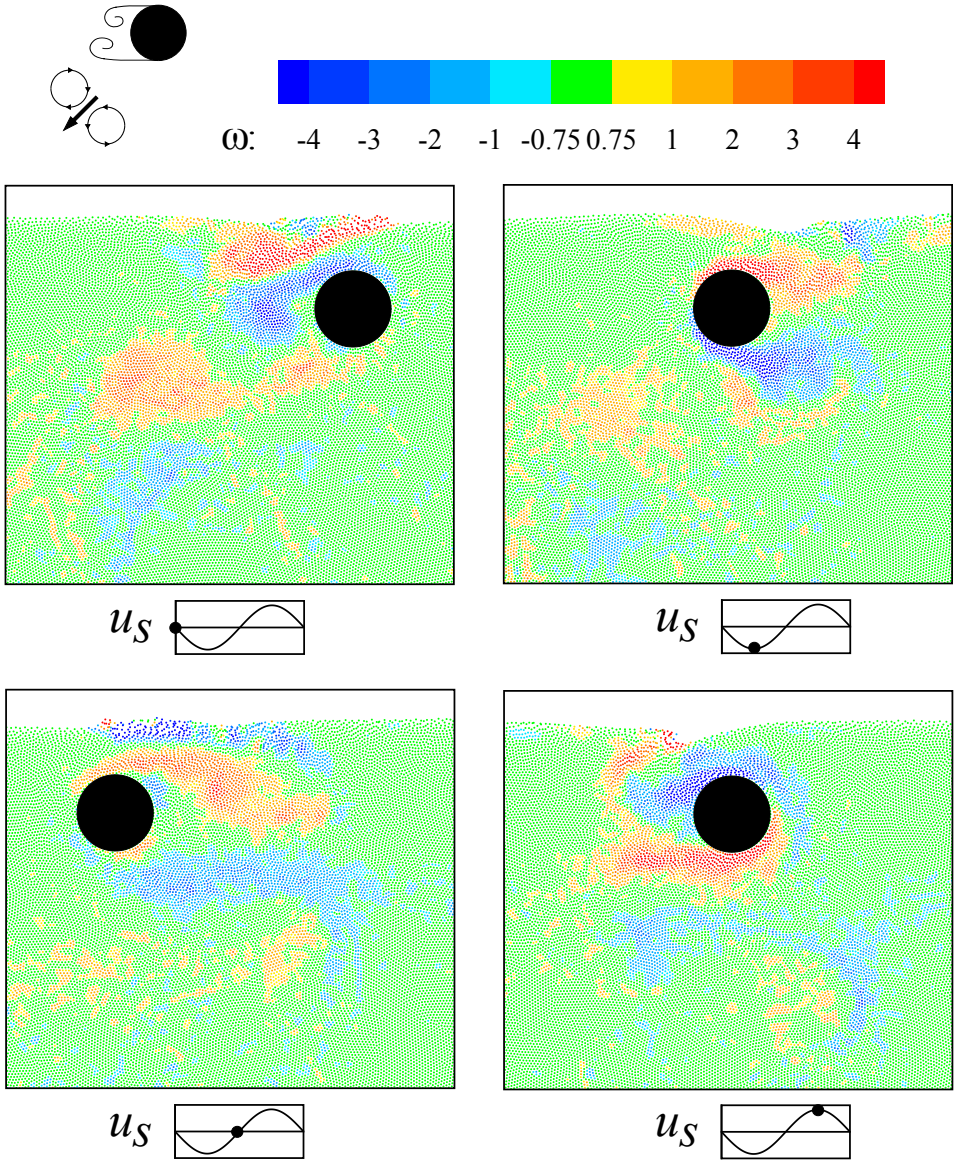

Figure 7. Instantaneous vorticity distribution predicted by the DFIB-SPH model at different times during the forced oscillation cycle of a horizontal cylinder beneath the free surface of a liquid for KC = 10 $H/D = 0.75$.

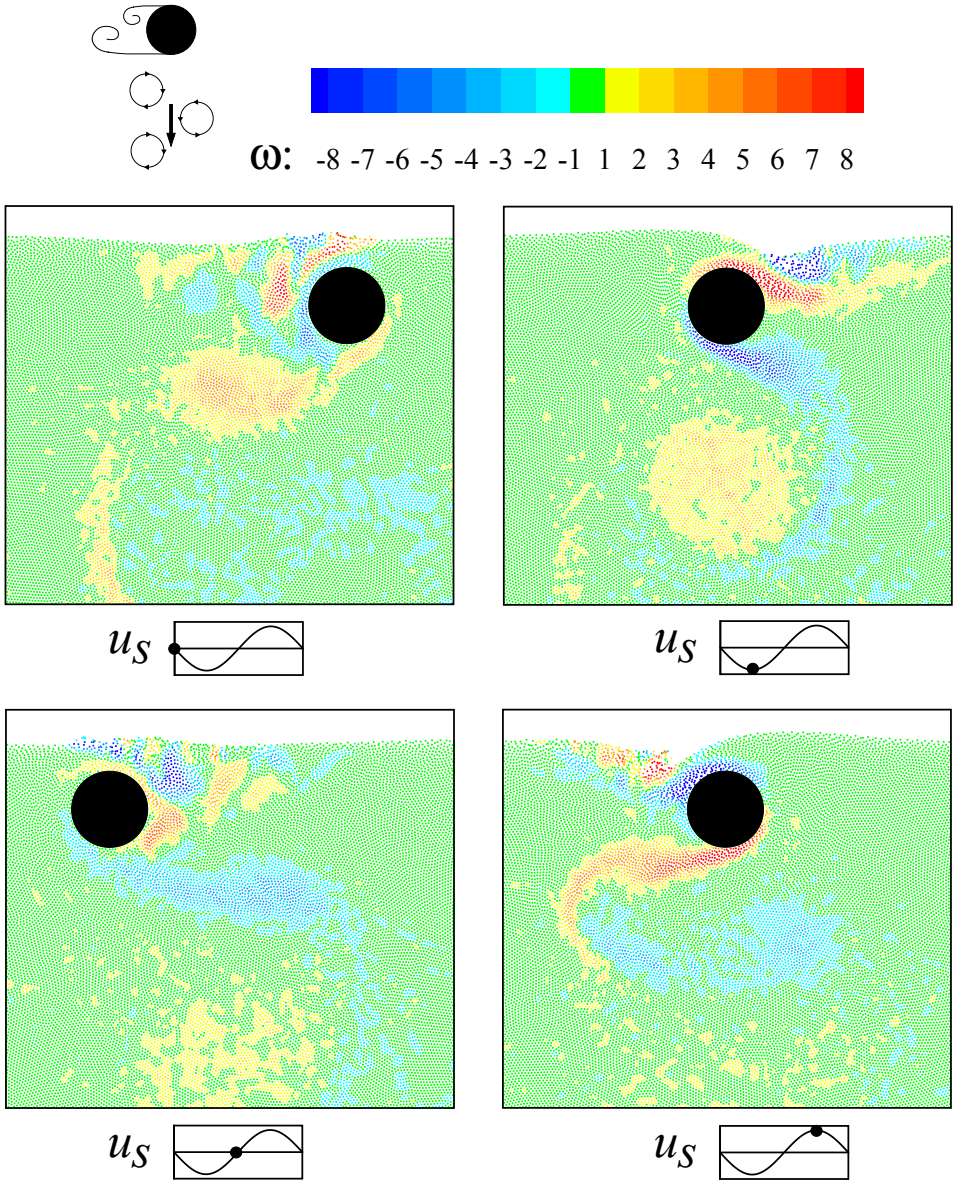

Figure 8. Instantaneous vorticity distribution predicted by the DFIB-SPH model at different times during the forced oscillation cycle of a horizontal cylinder beneath the free surface of a liquid for KC = 10 $H/D = 0.5$.

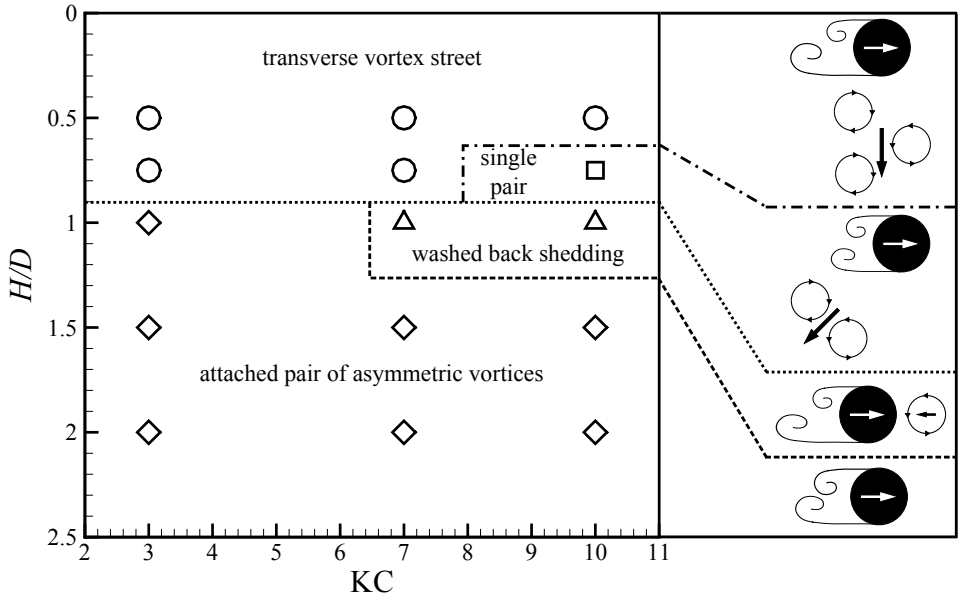

Figure 9. KC-H/D map indicating different classes of flow patterns obtained for a horizontal cylinder undergoing forced oscillation below the free surface of a liquid, predicted by the DFIB-SPH model.

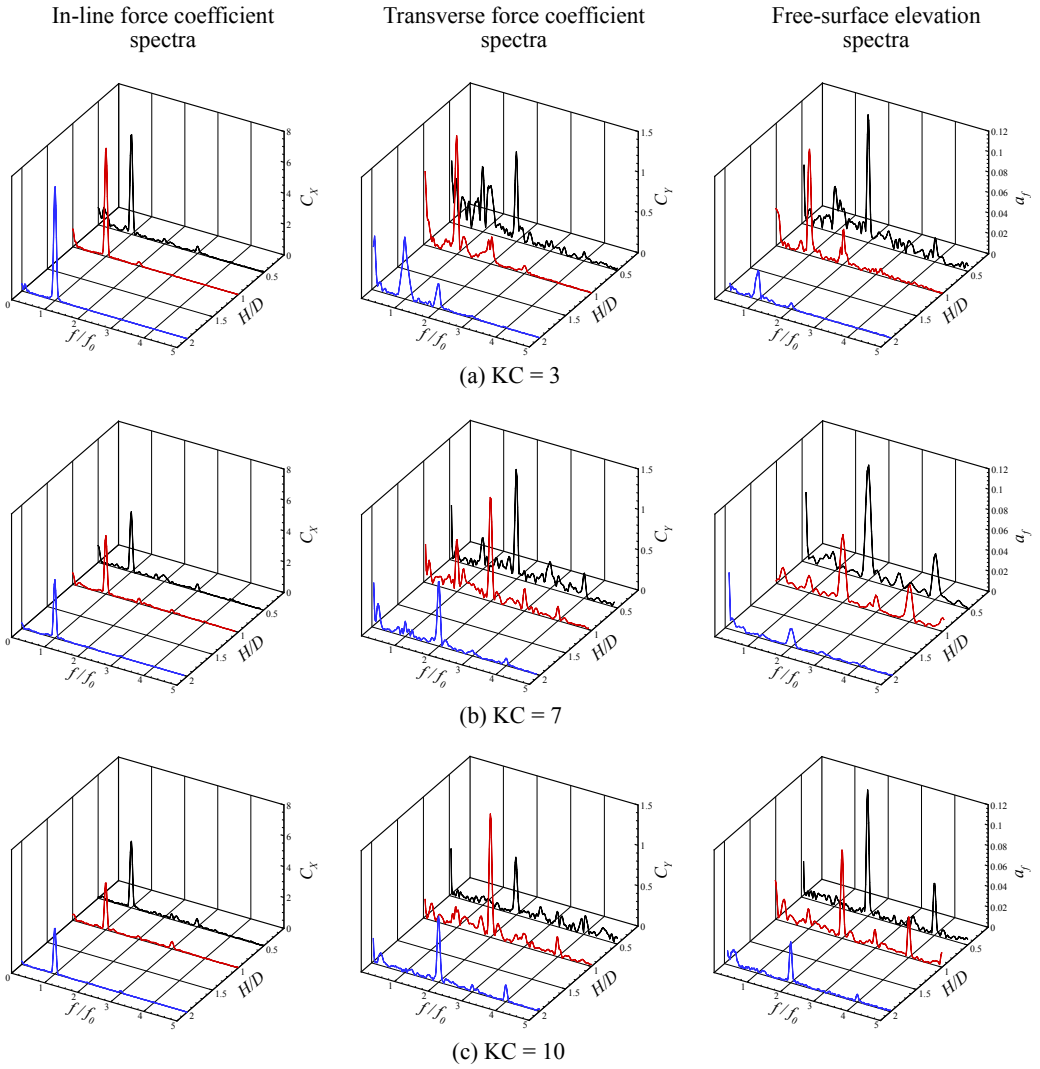

Figure 10. In-line force coefficient, transverse force coefficient, and free surface elevation spectra obtained for KC $= 3 - 10$, and submergence ratios of $H/D = 0.5 - 2$. Here f is frequency, and f_0 is the oscillation frequency.

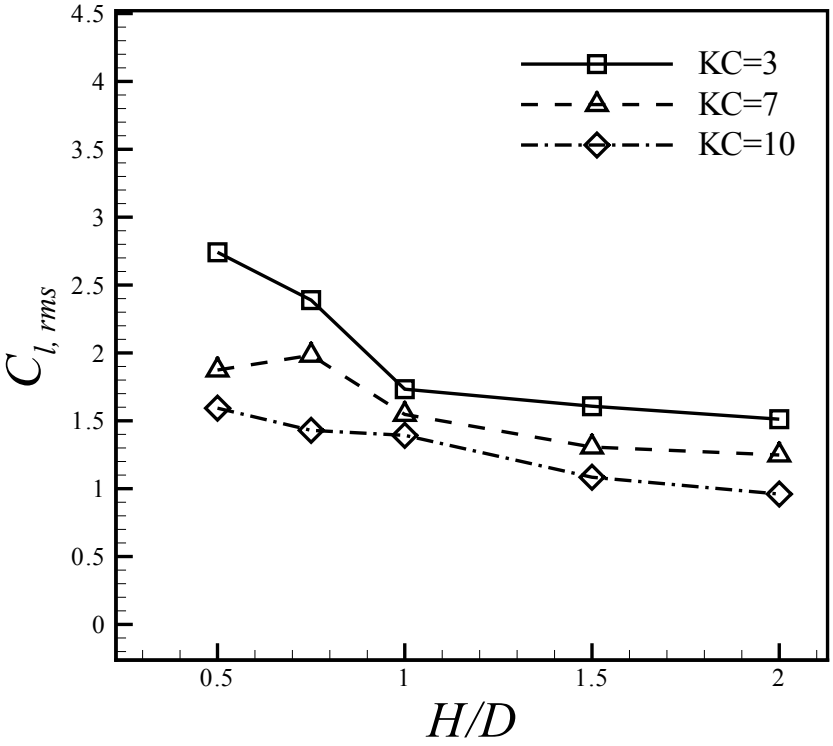

Figure 11. Root-mean-square values of transverse force coefficient obtained for KC = 3, 7, and 10, and submergence ratios of $H/D = 0.5 - 2$.

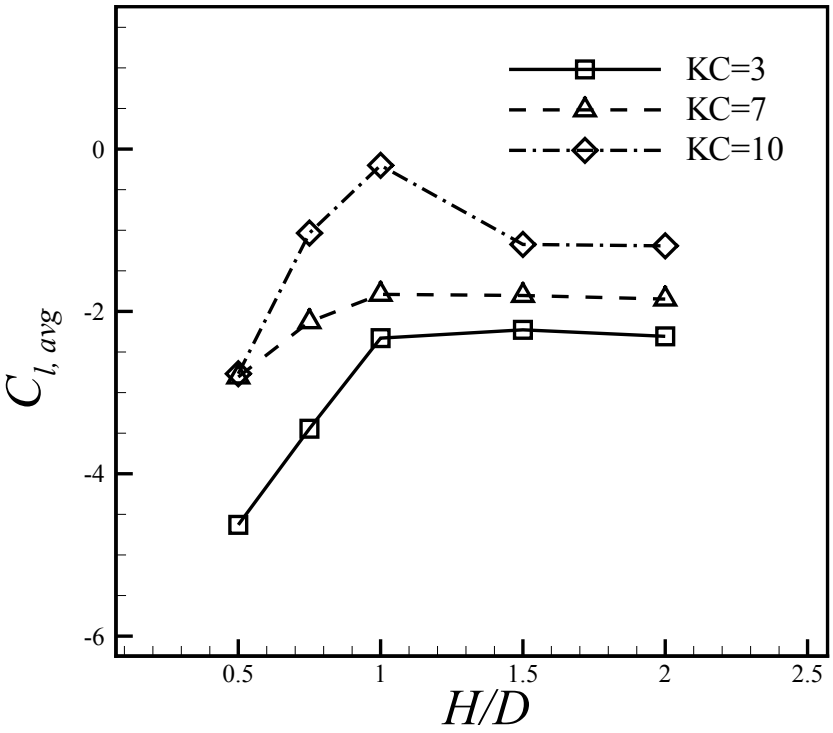

Figure 12. Average values of transverse force coefficient obtained for KC = 3, 7, and 10, and submergence ratios of $H/D = 0.5 - 2$.

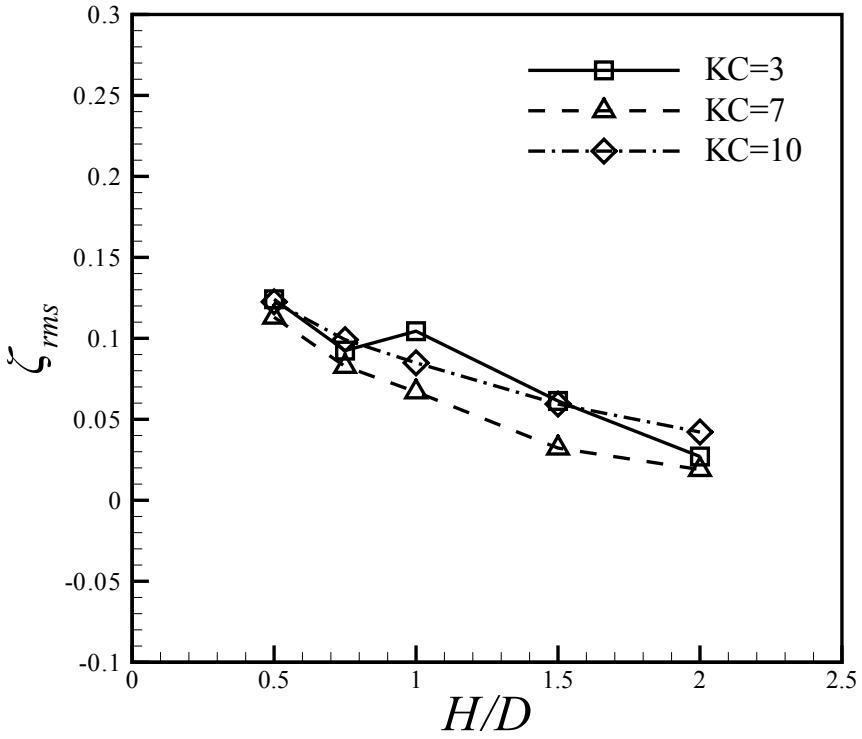

Figure 13. Root-mean-square values of free surface elevation obtained vertically above the mean position of the oscillating cylinder for KC = 3, 7, and 10, and submergence ratios of $H/D = 0.5 - 2$.